IL NUOVO CIMENTO Vol. 31 C, N. 5-6 Settembre-Dicembre 2008
DOI 10.1393/ncc/i2009-10354-3

Experimental measurements and diffusion in harbor and coastal zones

M. Diez([1]), M. O. Bezerra([2]), C. Mosso([1]), R. Castilla([3]) and J. M. Redondo([1])(*)

([1]) *Universitat Politecnica de Catalunya - Barcelona, Spain*
([2]) *Laboratório de Oceanografia Física (LOF), Faculdade de Oceanografia Instituto de Geociências do Mar (LABOMAR), Universidade Federal do Ceará (UFC) Fortaleza, Brazil*
([3]) *Universitat Politecnica de Catalunya - Terrasa, Spain*

(ricevuto il 10 Gennaio 2009; approvato il 10 Aprile 2009; pubblicato online il 17 Luglio 2009)

Summary. — Experimental results of turbulent flows in the sea surface near the coastline have been performed using both Lagrangian and Eulerian methods, field tests are presented using video recordings and velocity sensors. The spatial and temporal resolution is limited by the measuring instruments, which results in "filtering" out the very small scales. The experimental field-results obtained during the large-scale surf zone experiments carried out in the Ebro Delta, (Spain), under spilling/plunging breaking waves are compared with experiments performed at the Barcelona harbour. The field-measurements include several tests across the surf zone with high vertical resolution. The measured turbulent properties are compared with macroturbulence characteristics and length parameterisations. Diffusion is measured and related to the local velocity spectra so that a generalized Richardson law may be used.

PACS 92.10.Sx – Coastal, estuarine, and near shore processes.
PACS 92.10.A- – Circulation and currents.

1. – Introduction

As there are multiple processes at different scales that produce turbulent mixing in the ocean, thus giving a large variation of horizontal eddy diffusivities, we use a direct method to evaluate the influence of different ambient parameters such as wave height and wind on coastal dispersion. Measurements of the diffusivity are made by digital processing of images taken from video recordings of the sea surface near the coast. The use of image analysis allows to measure both spatial and temporal characteristics of wave fields, surface circulation and mixing in the surf zone, near wave breakers and inside harbours. Velocity measurements are also used to relate integral length scales to wave

(*) E-mail: redondo@fa.upc.edu

activity. The study of near-shore dispersion, with the added complexity of the interaction between wave fields, longshore currents and local turbulence need detailed measurements of mixing and diffusion if we want to understand the complexity of coastal dynamics. The measurements include simultaneous time series of waves, currents, wind velocities and profiles from the studied areas.

Quantitative information from the video images is accomplished using the DigImage video processing system, and a frame grabber on an IBM compatible computer, which allows a resolution of 512 by 512 pixels and 256 grey levels. The video may be controlled by the computer, allowing remote control of the processing. Spectral analysis on the images has also used in order to estimate dominant wave periods as well as the dispersion relations of dominant instabilities. The measurements presented here consist mostly on the comparison of diffusion coefficients measured by evaluating the spread of blobs of dye (milk) as well as by measuring the separation between different buoys released at the same time.

We have used a non-intrusive technique, developed by Diez [1-3], Rodriguez [4, 5], Bezerra [2, 3] and other authors [6-9] to study turbulent diffusion by means of digital processing of images taken from remote sensing and video recordings of the sea surface. The use of image analysis allows to measure variations of several decades in horizontal diffusivity values, but because of the many different conditions forcing the coastal flows the comparison of the diffusivities between different sites is not simple and a good understanding of the dominant mixing processes is needed. Measurements have been made near the coast in a series of field experiments at the Trabucador beach in the Ebro Delta, south of Barcelona in Vilanova i la Geltru, and inside of the Harbour of Barcelona. One of the clear differences between the measurements arise from the existence or not of a longshore current, which is absent in enclosed areas.

The measurements were performed under a variety of weather conditions and conditional sampling has been used to identify the different influences of the environmental agents on the actual effective horizontal diffusion and other relevant turbulence parameters (fig. 1).

Next we discuss turbulent diffusion, in sects. **3** and **4** we present Lagrangian and Eulerian coastal measurements and in **5** we compare the results with a kinematic simulation model and present the conclusions.

2. – Dispersion in the ocean surface

Horizontal mixing and momentum transport is indicated by the correlations between velocity and concentration of the dispersed agent (dye, temperature, density differences, etc.), or between different components of velocity.

The basic equation describing the behaviour of the concentration of a solute in time and space is the advection diffusion equation that may be simplified in one-dimensional form and furthermore if we consider the centre of reference as a moving one at the centre of mass of the solute or dispersed agent, c, then Fick's equation may be written as

$$\frac{\mathrm{d}c}{\mathrm{d}t} = -\frac{\mathrm{d}}{\mathrm{d}x}Fc = -\frac{\mathrm{d}}{\mathrm{d}x}\left(-D\frac{\mathrm{d}}{\mathrm{d}x}\right) = D\frac{\mathrm{d}^2c}{\mathrm{d}x^2}. \tag{1}$$

So that the ratio $\mathrm{d}c/\mathrm{d}t$ that measures locally the variation of concentration of the dispersed substance with time equals the diffusion coefficient times the Laplacian of c. (D is often reserved to denote the uniform molecular diffusivity.)

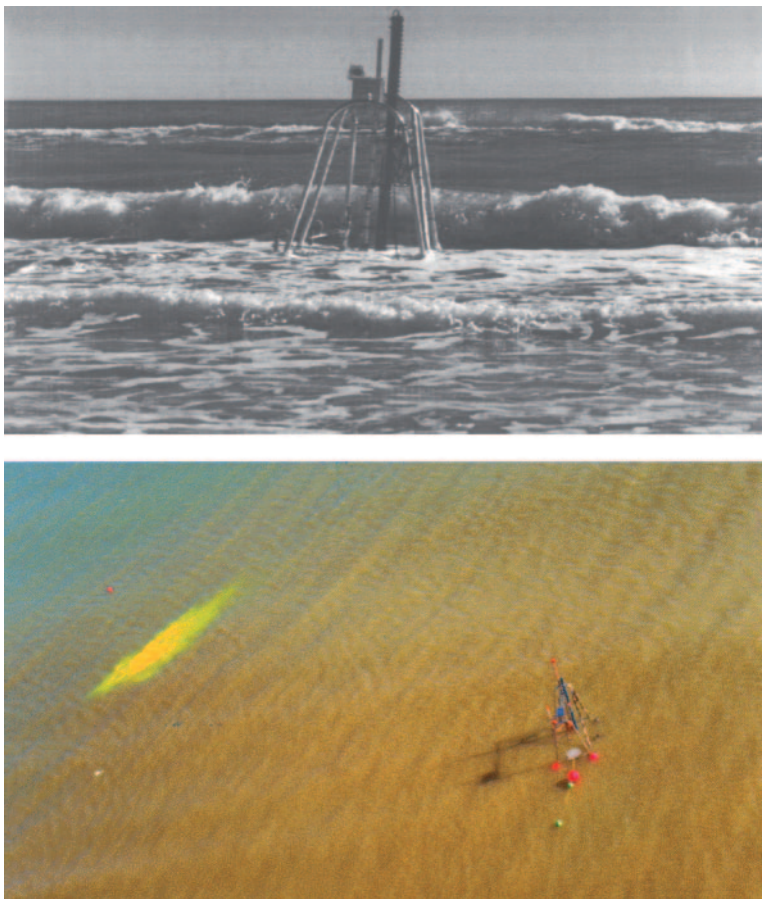

Fig. 1. – Instrumented carriage with wave gauges. 6 EM velocity meters and optical sediment sensors [4] (above), video measurement of a fluoresceine dye blob near the carriage (below).

For the turbulent diffusion, the simplest closure consists in assuming a similar turbulent diffusivity coefficient, $K(x,t)$, which may vary from point to point and in time, and often it is a tensor, when anisotropy is important. So the simplest turbulent diffusion equation uses Boussinesq scheme relating turbulent fluxes to concentration gradients;

$$\frac{\mathrm{d}c}{\mathrm{d}t} = \frac{\mathrm{d}}{\mathrm{d}x}\left(K(x,y,z,t)\frac{\mathrm{d}c}{\mathrm{d}x}\right) \qquad \text{so that} \qquad K = \overline{u'c'}\Big/\frac{\mathrm{d}c}{\mathrm{d}x}\,.$$

And considering both molecular and turbulent diffusivities we have

$$\frac{\mathrm{d}c}{\mathrm{d}t} = D\frac{\mathrm{d}^2c}{\mathrm{d}x^2} + \frac{\mathrm{d}}{\mathrm{d}x}\left(K(x,t)\frac{\mathrm{d}c}{\mathrm{d}x}\right). \tag{2}$$

In the case when a boundary, such as a wave breaker, transfers momentum to the coastal flow through horizontal shear the turbulent diffusivity $K(x,t)$ depends on the distance z. The same hypothesis used by Von Karman for the Atmospheric Boundary Layer may

be used, defining a relevant scale of velocity, that associated to the turbulent sidewise friction produced by the boundary as

$$\rho^{-1}\,\tau = {u_*}^2,$$

then, assuming that eddies proportional to the distance from the breaker are most efficient, we model the lateral shear as

$$\mathrm{d}U/\mathrm{d}z = u_*/kz, \tag{3}$$

κ being the so-called Von Karman constant with a value for the atmosphere of 0.41. Integrating the differential equation we have a logarithmic current profile such as

$$U(z) = u_* \ln(z/z_o)/\kappa. \tag{4}$$

Defining z_o as the small-scale sidewise friction length scale at which the mean lateral velocity is zero (but note that fluctuations may exist very close to the boundary). The well-known logarithmic profile would then be modified with other dimensional parameters if stratification or rotation are important. The Richardson number derived relating the buoyancy and the production terms in the turbulent energy equation is a measure of mixing efficiency. In the hypothesis of Reynolds, the turbulent mixing or transport coefficients for momentum and heat are supposed equal, because both seem diffused by similar eddies in the same way. But if there is appreciable stratification, this is not true, mostly due to the presence of internal waves. Which does not produce mixing.

In recent years a number of theoretical, numerical and experimental studies have been devoted to the understanding of non-homogeneous turbulent dynamics. Activity in this area intensified when the basic Kolmogorov self-similar theory was extended to two-dimensional or quasi-2D turbulent flows such as those appearing in the environment, both in the atmosphere and the ocean. The statistical description and the dynamics of these geophysical flows depend strongly on the distribution of long-lived organized (coherent) structures [10-12] as seen in figs. 2 and 3 from SAR satellite images.

The satellite-borne SAR seems to be a good system for detecting man-made oil spills and oil slicks dynamical features. It is also a convenient tool to investigate the eddy structures of a certain area where the effects of bathymetry and local currents are important in describing the ocean surface behaviour. In the example presented near Barcelona, the maximum eddy size agrees remarkably well with the limit imposed by the local Rossby deformation radius using the usual thermocline-induced stratification. The Rossby deformation radius, defined as $Rd = (N/f)h$, where N is the Brunt-Väisälä frequency ($N^2 = \frac{g}{\rho}\frac{\partial \rho}{\partial Z}$), f is the local Coriolis parameter ($f = 2\Omega \sin \Theta$, where Ω is the rotation of the Earth and Θ is the latitude) and h is the thermocline depth, is about 10–100 km.

The geometry of grey scale ranges and boundaries of spatial dynamic surface features may contain new helpful information by using multifractal analysis techniques to investigate oil spills, as in [13], and also in the application of these techniques to the analysis of ocean surface fractal features (eddies, mushroom-like currents, etc.).

3. – Lagrangian statistics

The overall results indicate that there is a strong dependence of horizontal eddy diffusivities on the wave Reynolds number as well as on the wind stress evaluated from

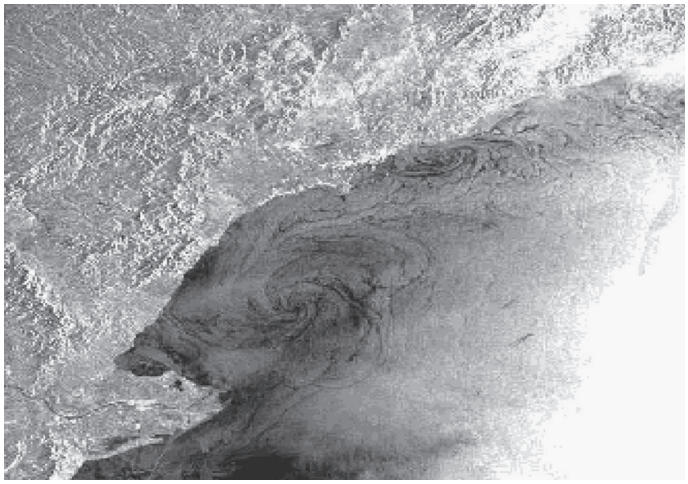

Fig. 2. – SAR image from ERS2 near the Ebro Delta (Platonov 2002).

the friction velocity from wind profiles measured at the coastline as indicated in Bezerra *et al.* [3, 4], but the present paper integrates also measurements inside harbours or at locations protected by wave-breakers. Both wind and wave effects are very important and give several decades of variation of eddy diffusivities measured near the coastline (between 0.0001 and $2\,\mathrm{m}^2/\mathrm{s}$), see fig. 4.

Longshore currents are also important near the coast and it is interesting to compare two similar sites with and without side harbours that hamper the longshore current formation. Experiments of dye diffusion such as those performed filming and video recording the evolution of slicks allow to characterize the ranges of K_x and K_y using

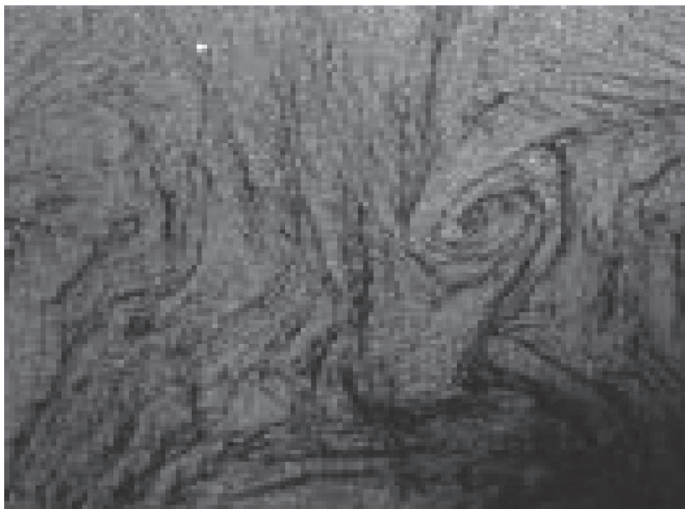

Fig. 3. – SAR images from ERS2, showing an elongated oil spill and vertical structures produced by Langmuir cells.

Fig. 4. – Video Image from the top of the crane at the experiments performed at Trabucador bar at the Ebro Delta [1-3].

Einstein's equation

$$K_i(x,y) = \frac{1}{2}\frac{\mathrm{d}{\sigma_i}^2(x,y)}{\mathrm{d}t}\,, \tag{5}$$

with $\sigma_i(x,y)$ a relevant dispersion length scale in the direction i.

These coefficients are a function of the distance to the coast and other environmental factors such as wave height and frequency, as shown in fig. 5, wind stress, tides and mean

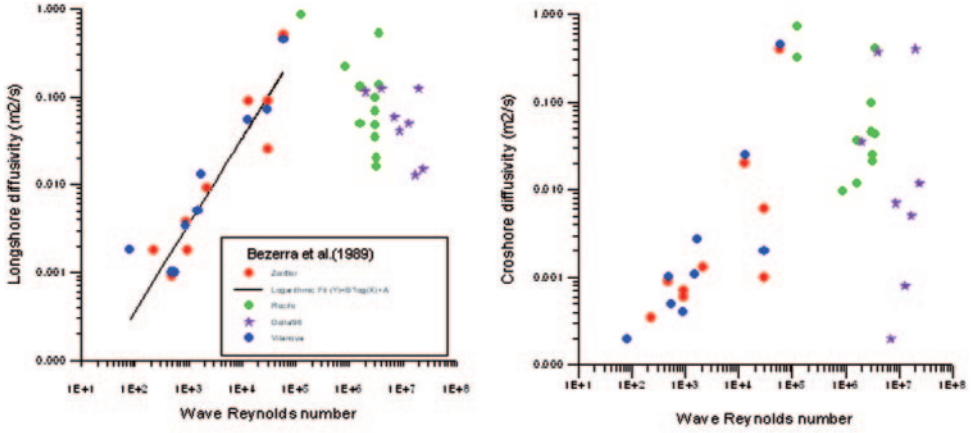

Fig. 5. – Values of the eddy diffusivity horizontal coefficients (Kx and Ky) as a function of wave Reynolds number, from Bezerra *et al.* [3].

currents, the particle trajectories can be used for the direct investigation of absolute and relative dispersion. In addition, Lagrangian descriptions of local flows are compared with Eulerian, single point measurements description, but care is needed when transforming Eulerian into Lagrangian measurements.

Let T be the total acquisition time and Δt the time interval between subsequent images; the position of a particle is known at a discrete series of times $t_j = j\Delta t$, $j = 1, \ldots, N$ where $N = T/\Delta t$. Each successful tracking of a particle gives a trajectory described by the vector [14]

$$\boldsymbol{X} = \boldsymbol{X}(m, j) \tag{6}$$

that indicates the position as a function of the particle m and of discrete time j. To identify the particles, it is advisable to use a progressive numeration.

In a Lagrangian framework, the large-scale characteristics of the fluid motion are described by Lagrangian integral time scale. The Lagrangian integral time scale T_L is a parameter that describes how long a fluid particle "remembers" its past. In other terms, the larger it is, the longer a particle will be affected by what occurs. From a theoretical point of view, it is defined as the integral of the auto-correlation coefficient, and for a discrete time series it is

$$T_{L,r}(\boldsymbol{X}) = \Delta t \sum_{n=0}^{\infty} \boldsymbol{r}_{rr}(\boldsymbol{X}, n). \tag{7}$$

Release time, $(t - t_0)$ is denoted by τ, and we have

$$c(\tau, z) = N(\tau) p(z|\tau, z_s). \tag{8}$$

The integrated concentration can be finally normalized by the uniform concentration

$$c_0(\tau) = \frac{N(\tau)}{z_i}\,, \tag{9}$$

so that the non-dimensional concentration field depends neither on the actual number of trajectories intersecting $z = z_s$ nor on their lengths. Assuming the hypothesis of frozen turbulence, the non-dimensional time $T = t/t^*$ can be transformed in non-dimensional downwind length, which may be identified with the *integral length scale* obtained also by Eulerian measurements of turbulent velocity in the coastal zone.

4. – Eulerian measurements near the coast

Electromagnetic sensors have been used to measure turbulent velocities and oscillatory flow in marine environments [3-5]. The electromagnetic sensors are based on Faraday's law of electromagnetic induction measuring the velocity of a conductive liquid moving through a magnetic field. The power supply frequency, jointly with the physical dimensions of the sensor, impose a theoretical upper limit on the instrument sensitivity (both size and frequency response). Their main advantages are robustness, tolerance to particles or air contamination and good frequency response in the range 5–20 Hz. The upper limit needs to be verified for each specific electromagnetic sensor type. Recent laboratory and field comparisons between the spherical-type (3.8 cm diameter) and the

TABLE I. – *Field-experiment conditions.* $(^{+})$ *for wave crests.*

Field test n.	Shore-line distance (m)	Depth (m)	Peak wave period (s)	$H_{\mathrm{r.m.s.}}$ (m)	$U_{\mathrm{orb\,r.m.s.}}{}^{(+)}$ (m/s)
F5	40.0	1.13	7.1	0.62	0.61
F6	25.0	0.67	7.1	0.53	0.57
F7	17.0	0.54	8.0	0.43	0.53
F8	45.5	1.35	7.1	0.53	0.44
F9	32.0	0.72	7.1	0.51	0.71
F10	25.0	0.71	7.1	0.40	0.51
F11	21.5	0.63	8.0	0.34	0.52
F12	12.0	0.40	8.0	0.21	0.52

disc-type (5.5 cm diameter head) current meters have shown 5 Hz and 10 Hz as valid upper frequencies [4-6]. The $VTM2$ sensors seem to work well up to 20 Hz. On the other hand, the ultrasonic sensors are based on the frequency changes of a sound beam propagating along a flow path. The flow velocity is estimated from the sound propagation velocity (typically 1500 m/s). The ultrasonic sensors have an excellent frequency response (up to 30 Hz), allowing 3D measurements, but are fragile and sensitive to particle/air contamination.

Near the Ebro Delta, located in the Spanish Mediterranean coast, fig. 2, Rodriguez *et al.* [4, 5] reported the DELTA'93 and 96 experiments, from which high-resolution hydrodynamic data were obtained and analysed. This surf-zone campaign took place along the Trabucador bar, a barred longshore-uniform sandy beach. The motivation for this campaign was the lack of detailed data on surf-zone hydrodynamics in uniform coastal environments. The experiments were thus focused on the three-dimensional structure of the flow, including different time-scales: *currents, oscillatory flow* due to wind waves, and *macroturbulence*. The discussion of field experiments and waves/currents modelling can be seen in [2-5].

The measured field data include bathymetry, shoreline features, wave data outside and inside the surf-zone, mean water levels across the surf-zone, and the associated horizontal and vertical velocity profiles. A mobile sledge (fig. 1) was used across the beach to register hydro and morphodynamic conditions across the surf-zone from the shoreline up to 2 m depth.

The vertical structure of horizontal velocities u, v was measured with six two-dimensional electromagnetic current meters (Delft p-S with a 4 cm diameter head), fixed on a sledge. The instrumental sledge had also 3 optical backscatters, a compass and an optical prism. The vertical spacing of the electromagnetic sensors ranges from 0.10 to 0.20 m, starting at 0.10 m above the bottom and up to 0.80 m above the bottom, with a helicoidal distribution and a sampling rate of 20 Hz. The velocity-error was less than 2.5 cm/s (1% of the full-scale range). Simultaneously, the local water level evolution was measured with a vertical step wave-gauge (*Etrometa*) at a sampling rate of 4 Hz.

During DELTA'93 experiments [4, 5], several tests were carried out, but in this paper only measurements corresponding to medium-high incident waves are presented. These tests show more clearly the macroturbulence features. The incident wave conditions are summarised in table I for the 8 selected tests. The root-mean-square wave height $H_{\mathrm{r.m.s.}}$

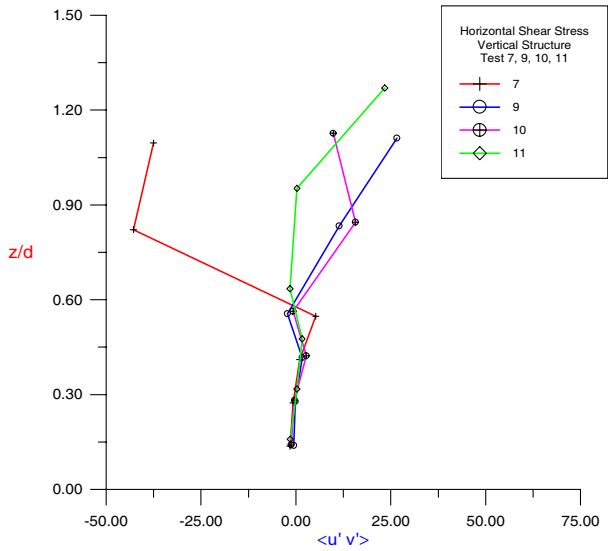

Fig. 6. – Vertical structure of horizontal shear stresses $\langle u'v' \rangle$ for tests 7-11.

and the mean water depth d correspond to 256 s time-series selected during maximum wave height conditions. On the other hand, to compare kinetic energies for oscillatory flow (waves), orbital velocities were obtained using a 4 Hz sampling rate. A conditional average of r.m.s. velocities under wave crests was performed for long 1200 s time series.

The horizontal turbulent intensities u', v' were obtained as the r.m.s. values of the filtered velocities,

$$u' = \sqrt{\frac{1}{n} \sum_{j=1}^{n} {u'_j}^2}, \tag{10}$$

where $u'_j = u_j - \bar{u}_j$, the fluctuating filtered velocity and n the length of the measured series ($n = 4120$).

The horizontal intensities (u', v') show values similar to previous studies in the middle and lower water column (approximately 0.01 of wave phase speed C). Near the wave-trough and free surface, turbulent intensities can increase up to 0.1 C. These upper values fall within the range of available laboratory data [8, 9, 15].

Inside the surf zone all intensities (tests 5-11) show a *parabolic* trend, which seems not to be sensitive to the cut-off frequency used to define the surf-zone macroturbulence. A different trend has been found near the swash zone (test 12), where the intensities show higher values and a *linear* profile. Figure 4 shows the cross-shore variation of u' scaled with the measured orbital velocity under wave crests. As discussed below, the values of the cross-shore r.m.s. components were larger than those of the long-shore component by a factor of 1.18 but showed similar profiles.

The vertical distribution of horizontal turbulent stresses $\langle u'v' \rangle$ is shown in fig. 6. It can be seen that $\langle u'v' \rangle$ is very important in the upper third of the water column, where the horizontal momentum transfer is expected to be vertically anisotropic and much higher near the water surface. This is important for the correct parameterisation of

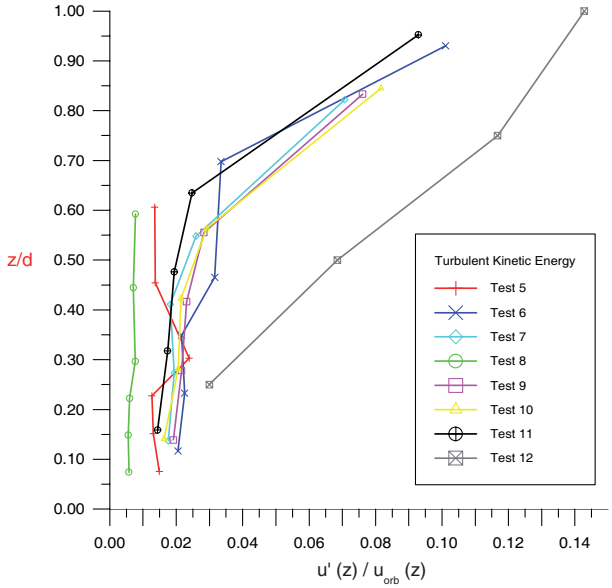

Fig. 7. – Kinetic energy k for all tests.

numerical models, where the eddy viscosity profile should have a strong vertical variation as observed.

The determination of the turbulent length scales ($\mathcal{L}$) is important to estimate the eddy viscosity ν_t that is in turn used for modelling hydrodynamics, sediment transport and pollutant dispersion inside the surf zone. In this work, the classical definition of the integral length scale of the turbulence $\mathcal{L}$ is used:

$$\mathcal{L} = \int_0^{L_{\max}} \langle u'_j \cdot u'_{j+dL} \rangle \mathrm{d}L, \tag{11}$$

where the horizontal turbulent velocity ($u' = (u'^2 + v'^2)^{1/2}$) cross-correlation coefficients were computed for different sensor distances ($\mathrm{d}L$). The values of the spatial lags were fixed and obtained from the spatial separation in the sledge of the 6 electromagnetic sensors (16 values between 0.2 and $L_{\max} = 1.2\,\mathrm{m}$). The cross-correlations were smoothed before the application of eq. (11), see figs. 7 and 8 where the results for tests 7-15 are shown.

From these values a multiple regression was obtained using the depth-scaled r.m.s. wave height, non-dimensionalized with the water depth, and the Froude-scaled r.m.s. orbital velocity U_{orb} under wave crest, as independent variables,

$$\mathcal{L}/d = \alpha_1 + \alpha_2 H_{\mathrm{r.m.s.}}/d + \alpha_3 U_{\mathrm{orb}}/C, \tag{12}$$

where C is the local wave phase speed. The results are shown in fig. 9, which may be used in conjunction with Lagrangian diffusivity measurements.

The multiple regression parameters for the turbulent length scale in the surf zone were $\alpha_1 = 0.28$, $\alpha_2 = -0.84$ and $\alpha_3 = 2.82$; with a R^2 value for the fit of 0.95.

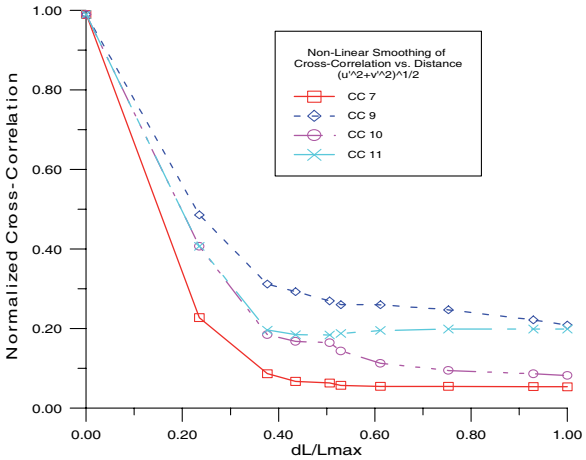

Fig. 8. – Integral length scales $\mathcal{L}$ curves for tests 7, 9, 10 and 11.

5. – Results at different sites and scales

There is an increase of diffusivity with wave height but only for large wave Reynolds numbers. Other important factors are wind speed and tidal currents. The horizontal diffusivity shows a marked anisotropy as a function of wave height and distance from the coast. A method for evaluating mesoscale eddy diffusivities in the ocean from the measured distribution of integral length scales and the eddy turnover times associated to inertial oscillations associated to the local Coriolis parameter $f(y)$ is discussed. Using the integral length scale distribution $l(x, y)$ we may calculate the large-scale eddy diffusivity as $K(x, y) = l(x, y)^2 f(y)$, where $K(x, y)$ is the horizontal diffusivity at latitude y and

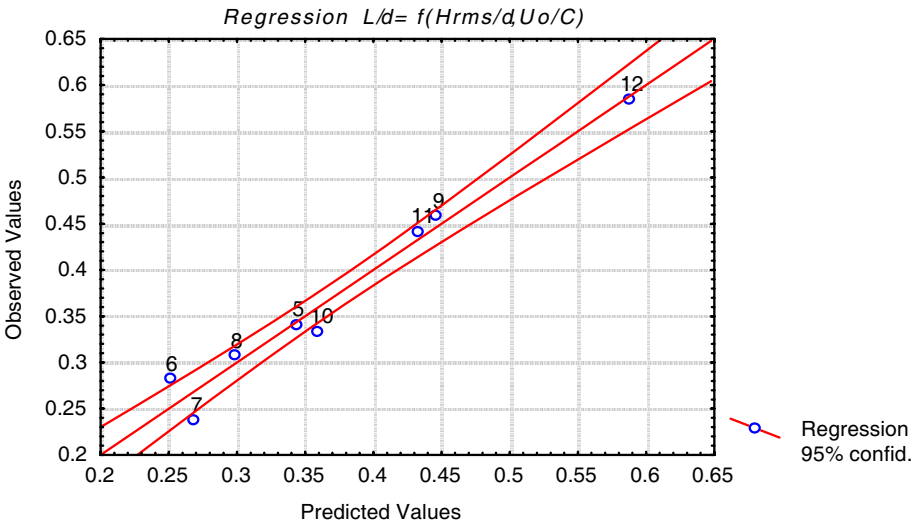

Fig. 9. – Multiple regression for dimensionless integral length scale $\mathcal{L}/d$.

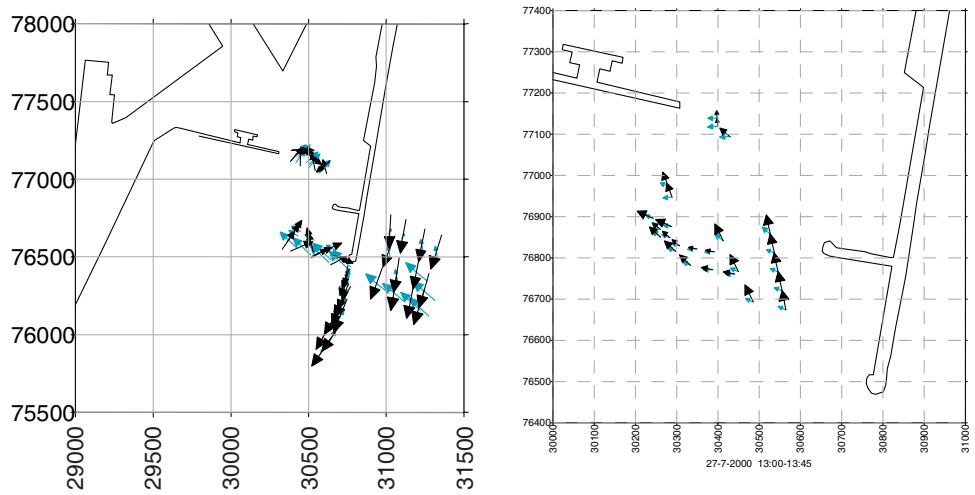

Fig. 10. – Lagrangian buoy and dye dispersion measurements at the Barcelona Harbor, the patterns are very dependent on the wind direction.

longitude x. A further refinement takes into account the multifractality of the images and the relation between fractal dimensions and velocity spectra. We will compare field measurements in open beaches and in harbours comparing Lagrangian statistics (see sect. **3**) in order to study and forecast pollutants dispersion. The results of a numerical model calculating diffusion from both DNS and kinematic simulation (KS) of a 2D turbulent fow is also presented. These flows which can be considered comparable to a geophysical flow akin to the sea surface flow [16, 17]; in this case, relative diffusion has been investigated, and experiments and simulations will be compared with respect to Richardson's law, that states that the area increase is proportional to the cube of the time:

$$\sigma^2(x, y) = ct^3. \tag{13}$$

Video digitizing of field events and remote-sensing image analysis seems a very promising technique for extended quantitative measurements of sea surface behaviour including the effects of different coastal instabilities, and allows to describe in more detail the coastal and platform zone. The local characteristics may give differences in horizontal diffusivities of more than a decade. The measurements in enclosed areas show in general smaller eddy diffusivity values (figs. 10 and 11), and most of the times the growth of the area is smaller than the cube of the time.

In open beaches the variation is larger, even reaching hyperdiffusivity. Closer to the shore, the non-linear effect of the surf zone is apparent in enhanced images. There is a process of wave dislocations, between the surf and the swash zones that needs further study. This produces a strong cross-shore variation of the eddy diffusivity values exhibiting a maximum between the first bar and the shore.

For example, if we assume that the standard turbulence spectrum has a well-defined shape over a significant range of scales or frequencies,

$$E(k) = k^{-m}, \tag{14}$$

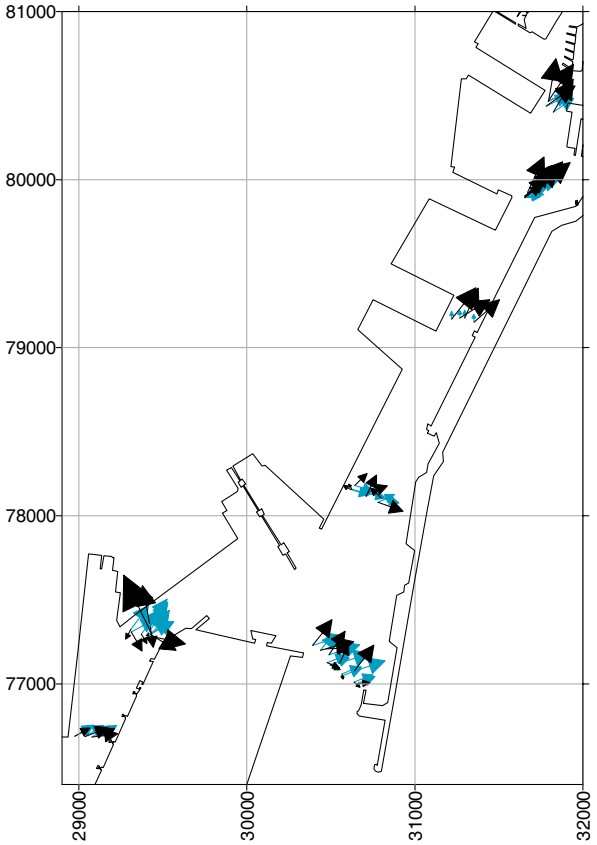

Fig. 11. – Surface velocity measurements inside the Barcelona Harbor.

where $E(k)$ is the spectrum function of the wave number $k = 2\pi/\lambda$. Here m is an exponent that in fully developed 3D turbulence is 5/3 but may take other values depending on the 2D or 3D characteristics of the cascade process and on the intermittency (related to the structure functions scaling laws). From eq. (13) we may generalize the possible time evolution of the dispersed area so that

$$\sigma^2(x, y) = ct^{\beta}. \tag{15}$$

The results may be also interpreted using a kinematic simulation model to investigate the role of different espectral cascade processes at the smallest scales down to the Batchelor scales [16]. The generalized Richardson's law consists in supposing that the relative dispersion D^2 of two particles in a turbulent flow varies in time as $D^2 \sim t^{\beta}$, and then find out the relationship between β and m. Fung and Vassilicos [18] found out, by dimensional analysis, supposing that the relative dispersion D^2 is only a local function of the energy spectra $E(D)$, this means that only eddies of the size of what is being dispersed are relevant for the dispersion; then this length, which is close to the integral lenth scale may be related to m as

$$D^2 \sim t^{4/(3-m)}. \tag{16}$$

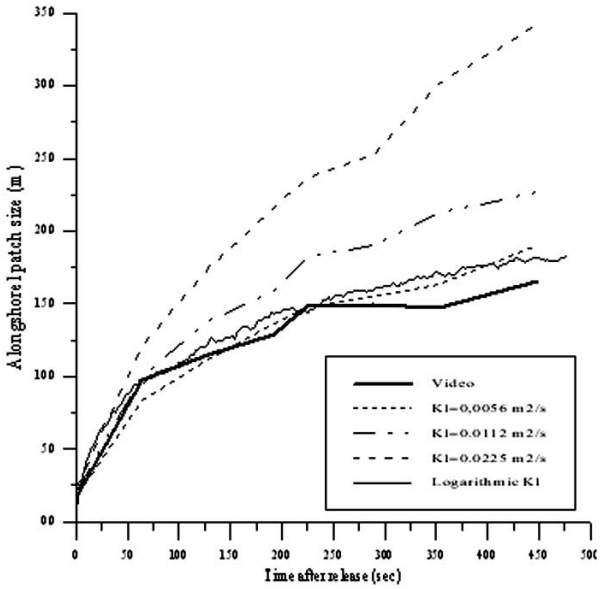

Fig. 12. – Example of the growth of dye patches in time, the slope of each experiment can be used to measure the local eddy diffusivity $K(x, y)$.

But as argued by them and shown by Castilla [16], for $m > 3$, the experimental results do not match with this theoretical formula, but rather stabilize towards a constant 4-8 depending on whether the total energy is maintained constant or just the energy of the integral scales is maintained constant.

Local eddy characteristics strongly influence the turbulent horizontal diffusivity, $K(x, y)$. As an example from [6], fig. 12 shows a map of local average diffusivities derived from SAR observations near Barcelona, of course Richardson's law has to be applied and different sizes of spills will also comply with the 4/3 law. Both numerical simulations [16-18] such as those shown in figs. 13 and 14, and laboratory experiments

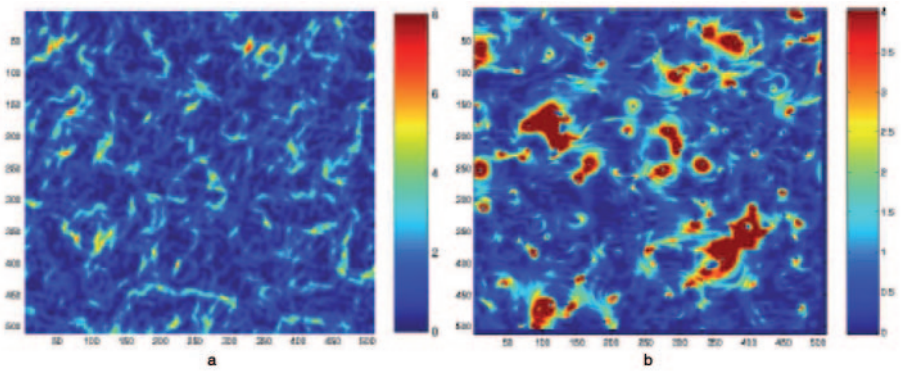

Fig. 13. – Comparison of a KS and DNS of the same spectra, local energy is plotted.

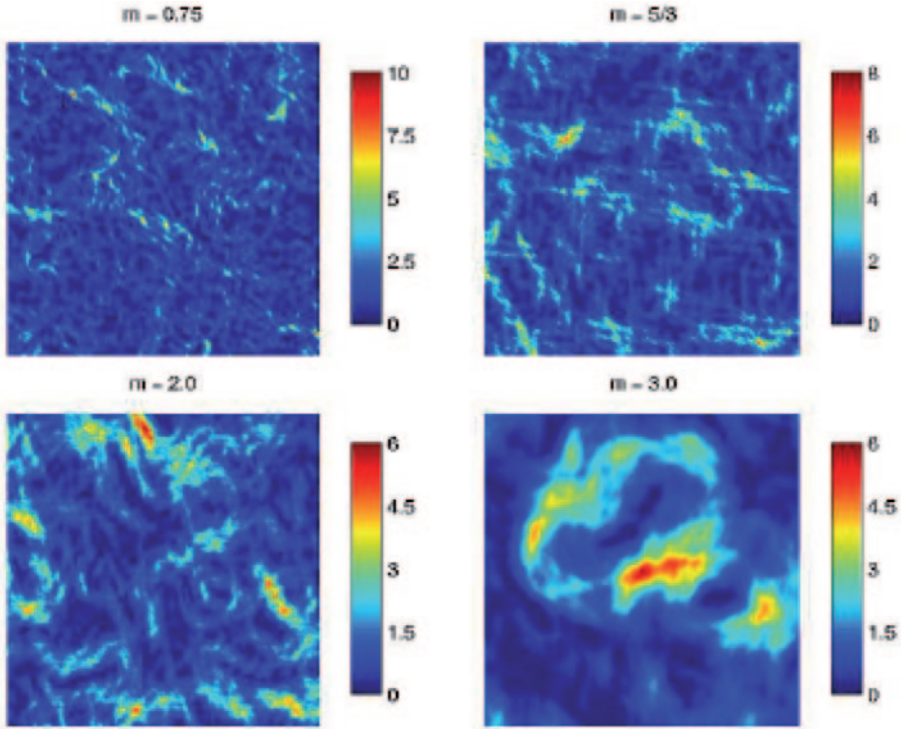

Fig. 14. – Distribution of energy for different KS with different spectral power laws. The integral length scales $\mathcal{L}$ clearly increase with higher m.

confirm the conditions for hyperdiffusion

$$\left(D^2 = ct^{\beta(f,N)} \quad \text{with } \beta(f,N) > 3\right) \tag{17}$$

to exist, as well as the trapping associated with coherent structures and vortices in the ocean, which are well detected under the Lagrangian video measurements.

Many of these image analysis techniques, that have been used extensively in laboratory investigation of the structure of turbulence, may be extended and used in satellite and field measurements [17-19]. These techniques allow the determination of the instantaneous and time-evolving spatial coherent structures of the flow. If we need detailed information of the flow, which is often the case for geophysical turbulent flows, the feature concentration must be high so that the spatial distances between the features are smaller than the smallest spatial scale of the flow. With SAR images the scale is cut off by the pixel resolution, but higher-resolution video images. For high feature densities the individual features between subsequent images cannot be recognised and therefore the feature displacements must be analysed by means of statistical data analysis techniques. Therefore, the image is subdivided in small areas (interrogation regions). Within each interrogation region the mean displacements of the features are calculated by estimating the (auto) covariance function of the grey values of the image.

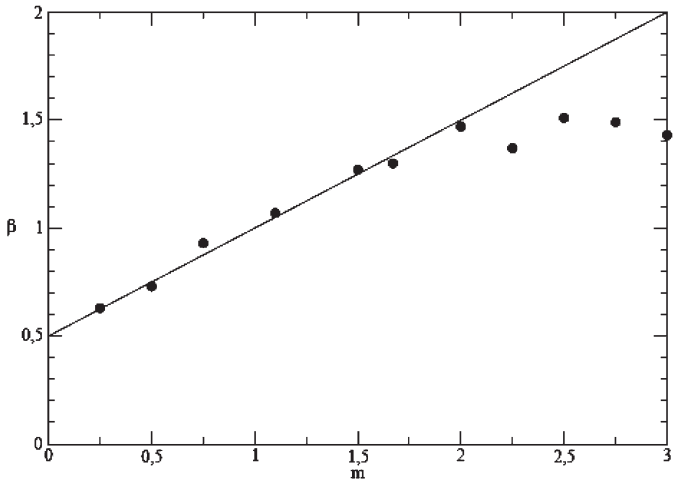

Fig. 15. – Empirical relationship between the slope of the power spectra and the time dependence of a tracer expension simulated with different KS with different spectral power laws.

6. – Conclusions

A good estimate of the eddy diffusivity comes from a scaling that includes the thickness of the surf zone as well as the depth and the wave period. Measurements in the Mediterranean are almost two orders of magnitude smaller than in the Pacific coast. On a larger scale, and further away from the coast the relevant eddy diffusivities are much larger, because large eddies often scale on the Rossby deformation radius, L_R.

Direct measurements of the diffusion and the horizontal velocity field were performed at several sites in the coastal areas of Spain. The diffusion coefficients were calculated by evaluation from video images of the area of milk and fluoresceine blobs released at different positions and with different wave heights, wind speeds and tidal induced currents. There are instances with either low diffusivity or hyperdiffusivity and local measurements in both cases indicate that spectra deviate strongly from an equilibrium spectrum. A generalized Richardson law such as that shown in fig. 15 from KS numerical models may be applied to coastal diffusion.

A non-homogeneous vertical structure for turbulence in the surf zone has been observed. This suggests the need of depth-varying models for a proper description of surf-zone hydrodynamics. The eddy viscosity values show a parabolic vertical distribution, where much higher values of eddy viscosity are restricted to the upper third of the depth. This behaviour does not occur near the swash zone where the variation of eddy viscosity with depth seems to be linear. This marked difference is probably due to the higher downward entrainment of surface-induced turbulence in the swash zone.

The local equilibrium assumption for surf zone turbulence is confirmed, since the turbulent dissipation is only important in the upper third of the water column, showing that the turbulent energy is mainly dissipated where it is produced. The results of more than 100 experiments show that there is a dependence of the maximum diffusivity on a Reynolds number derived from the wave height. There is an increase of diffusivity with wave height but only for large wave Reynolds numbers. Other important factors are wind speed and tidal currents. The horizontal diffusivity shows a marked anisotropy as

a function of wave height and distance from the coast. The diffusivity is also proportional to the friction velocity of the wind but shows a strong dependence on the position of the release, with a maximum at halfway between the shoreline and the position of the dominant sand bar. This behaviour is dominant when there is a strong longshore current present. The tidal induced dispersion is not easily parametrized, showing that even a generalized Richardson law such as that shown in eq. (16) is too simple.

* * *

We would like to acknowledge financial support both from (ERCOFTAC) and the CCD, Centre de Cooperacio i Desenvolupament of the UPC for a grant, we thank also the (ENV4-CT96-0334) European Union Projects ISTC1481, ESA-IP2240 and ESP2005-07551 for the SAR images provided and the Barcelona Harbour Authority for their support. Thanks are due to A. Babiano, A. Platonov and J. Vila.

REFERENCES

[1] Diez M., *Estudio de la Hidrodinamica de la zona de rompientes mediante el analisis digital de imagenes*, Master Thesis, UPC, Barcelona (1998).
[2] Bezerra M. O., *Diffusion de contaminantes en la costa*, PhD Thesis, Univ. de Barcelona, Barcelona (2000).
[3] Bezerra M. O., Diez M., Medeiros C., Rodriguez A., Bahia E., Sanchez-Arcilla A. and Redondo J. M., *J. Flow Turb. Combust.*, **59** (1998) 127.
[4] Rodriguez A., Sanchez-Arcilla A., Redondo J. M. and Mosso C., *Exp. Fluids*, **27** (1999) 31.
[5] Rodriguez A., Sanchez-Arcilla A., Redondo J. M., Bahia E. and Sierra J., *J. Water Science and Technology, IAWQ* (1995) 169.
[6] Artale V., Boffetta G., Celani A., Cencini M. and Vulpiani A., *Phys. Fluids*, **9** (1997) 3162.
[7] Boffetta G. and Celani A., *Physica A*, **280** (2000) 1.
[8] Lippmann T. and Holman R., *J. Geophys. Res.*, **94** (1989) 995.
[9] Sonu C., *Am. Soc. Photogram., Tech. Rep.*, **66** (1969) 91.
[10] Carrillo A., Sanchez M. A., Platonov A. and Redondo J. M., *Phys. Chem. Earth B*, **26/4** (2001) 305.
[11] Redondo J. M., Sanchez M. A. and Castilla R., *Vortical structures in stratified turbulent flows*, in *Turbulent Diffusion in the Environment*, edited by Redondo J. M. and Babiano A. (FRAGMA, Madrid) 2000, pp. 113-120.
[12] Redondo J. M. and Cantalapiedra I. R., *Appl. Sci. Res.*, **51** (1993) 217.
[13] Gade M. and Redondo J. M., *Marine pollution in European coastal waters monitored by the ERS-2 SAR: A comprehensive statistical analysis. IGARSS 99. Hamburg*, v. III (1999), p. 308.
[14] Monin A. S. and Yaglom A. M., *Statistical Fluid Mechanics: Mechanics of Turbulence*, Vol. **1** (The MIT Press, Cambridge, Massachusetts), 1971, p. 769.
[15] Hanna S. R., *J. Appl. Meteorol.*, **20** (1981) 242.
[16] Castilla R., *Simulación cinemática de flujo turbulento. Aplicación al estudio de la estructura de la turbulencia y la dispersión turbulenta*, PhD Thesis UPC, Barcelona (2001).
[17] Castilla R., Redondo J. M., Gamez-Monterol P. J. and Babiano A., *Nonlinear Processes Geophys.*, **14** (2007) 139.
[18] Fung J. and Vassilicos J. C., *Phys. Rev. E*, **52** (1998) 1677.
[19] Redondo J. M. and Platonov, *Environ. Res. Lett.*, **4** (2009) 14008.